Supplemental Information

Supplementary References

1. Gogolla N, Leblanc JJ, Quast KB, Sudhof TC, Fagiolini M, Hensch TK. Common circuit defect of excitatory-inhibitory balance in mouse models of autism. Journal of neurodevelopmental disorders. 2009;1(2):172-81. Epub 2010/07/29.
2. Selby L, Zhang C, Sun QQ. Major defects in neocortical GABAergic inhibitory circuits in mice lacking the fragile X mental retardation protein. Neuroscience letters. 2007;412(3):227-32. Epub 2007/01/02.
3. Fukuda T, Itoh M, Ichikawa T, Washiyama K, Goto Y. Delayed maturation of neuronal architecture and synaptogenesis in cerebral cortex of Mecp2-deficient mice. Journal of neuropathology and experimental neurology. 2005;64(6):537-44. Epub 2005/06/28.
4. Sadakata T, Washida M, Iwayama Y, Shoji S, Sato Y, Ohkura T, et al. Autistic-like phenotypes in Cadps2-knockout mice and aberrant CADPS2 splicing in autistic patients. The Journal of clinical investigation. 2007;117(4):931-43. Epub 2007/03/24.
5. Penagarikano O, Abrahams BS, Herman EI, Winden KD, Gdalyahu A, Dong H, et al. Absence of CNTNAP2 leads to epilepsy, neuronal migration abnormalities, and core autism-related deficits. Cell. 2011;147(1):235-46. Epub 2011/10/04.
6. Powell EM, Campbell DB, Stanwood GD, Davis C, Noebels JL, Levitt P. Genetic disruption of cortical interneuron development causes region- and GABA cell type-specific deficits, epilepsy, and behavioral dysfunction. The Journal of neuroscience : the official journal of the Society for Neuroscience. 2003;23(2):622-31. Epub 2003/01/21.

7. Gant JC, Thibault O, Blalock EM, Yang J, Bachstetter A, Kotick J, et al. Decreased number of interneurons and increased seizures in neuropilin 2 deficient mice: implications for autism and epilepsy. Epilepsia. 2009;50(4):629-45. Epub 2008/07/29.
8. Tripathi PP, Sgado P, Scali M, Viaggi C, Casarosa S, Simon HH, et al. Increased susceptibility to kainic acid-induced seizures in Engrailed-2 knockout mice. Neuroscience. 2009;159(2):842-9. Epub 2009/02/03.
9. Gogolla N, Takesian AE, Feng G, Fagiolini M, Hensch TK. Sensory integration in mouse insular cortex reflects GABA circuit maturation. Neuron. 2014;83(4):894-905. Epub 2014/08/05.
10. Meyer U, Nyffeler M, Yee BK, Knuesel I, Feldon J. Adult brain and behavioral pathological markers of prenatal immune challenge during early/middle and late fetal development in mice. Brain, behavior, and immunity. 2008;22(4):469-86. Epub 2007/11/21.
11. Stephenson DT, O'Neill SM, Narayan S, Tiwari A, Arnold E, Samaroo HD, et al. Histopathologic characterization of the BTBR mouse model of autistic-like behavior reveals selective changes in neurodevelopmental proteins and adult hippocampal neurogenesis. Molecular autism. 2011;2(1):7. Epub 2011/05/18.

Supplementary Tables

Supplementary Table S1. Mouse ASD models with reported altered PV immunoreactivity

Protein / Gene or Treatment	PV staining/ PV^+ number	Age (months)	Ref.
neuroligin 3 $Nlgn3^{R451C}$	Asymmetric "patchy" PV-deficit in cortex	2-3	(1)
fragile X mental retardation $Fmr1^{-/-}$	PV^+ neurons reduced in neocortex	≈ 12	(2)
methyl CpG binding protein 2 $Mecp2^{-/-}$	At PND15 no PV^+ cells	0.5 and 1.5	(3)
Ca^{2+}-dependent secretion activator 2 $Cadps2^{-/-}$	Reduction in PV^+ neurons in motor cortex and hippocampus	0.5	(4)
contactin associated protein-like 2 $Cntnap2^{-/-}$	Reduction in PV^+ neurons in striatum and cortex	0.5	(5)
plasminogen activator, urokinase receptor Plaur-/-	Reduction in PV^+ neurons	> 3	(6)
neuropilin 2 Nrp2-/-	Reduction in PV^+ neurons in hippocampus (CA1, CA3)	> 2	(7)
engrailed 2 En2-/-	PV „staining markedly reduced"	> 2	(8)
Shank 3 Shank3-/-	Relative intensity and size of PV^+ puncta surrounding pyramidal cells decreased in insular cortex	"adult"	(9)
Valproic acid (VPA) Treatment	Asymmetric PV deficit in cortex/hippocampus	2-3	(1)
Prenatal immune challenge (PolyI:C)	Reduction in PV^+ neurons in prefrontal cortex	6	(10)
BTBR inbred (C57BL/6J)	Reduction in PV-staining in anterior cingulate cortex	≈ 3 - 4	(11)

Supplementary Table S2. Properties of excitatory cortical inputs on FSI from $PV^{+/+}$, $PV^{+/-}$ and $PV^{-/-}$ mice. EPSC were evoked from the cortex and recorded in FSI in perforated-patch configuration. All the parameters were measured in voltage clamp. Data are presented as means±SEM. No significant differences were observed between genotypes.

	WT	PV+/-	PV-/-	*p*
N	11	8	12	
EPSC Amplitude (pA)	-162.17 ± 49.72	-125.92 ± 35.27	-164.88 ± 34.08	NS
Synaptic Delay (ms)	2.72 ± 0.14	2.59 ± 0.13	2.88 ± 0.14	NS
Rise Time 10-90% (ms)	2.42 ± 0.15	2.21 ± 0.24	2.17 ± 0.16	NS
Decay Time, τ (ms)	7.2 ± 0.48	5.97 ± 0.91	6.94 ± 0.78	NS
Variance/Mean (pA)	-5.53 ± 0.81	-6.18 ± 0.73	-8.62 ± 1.31	NS

Supplementary Figures

Supplementary Figure S1

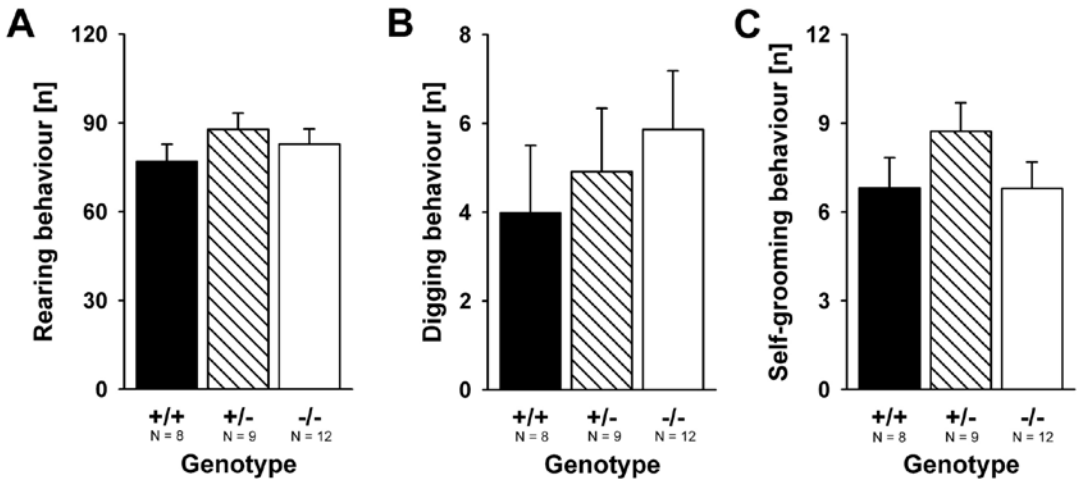

Supplementary Figure S1: No alterations in non-social behavior. $PV^{-/-}$ null mutant and $PV^{+/-}$ heterozygous mice do not display alterations in non-social behavior reciprocal social interactions as juveniles. (A) Total number of rearing behavior, (B) digging behavior, (C) and self-grooming behavior during the 5 min social interaction period. Data are presented as means±SEM, bars denoting SEM.

Supplementary Figure S2

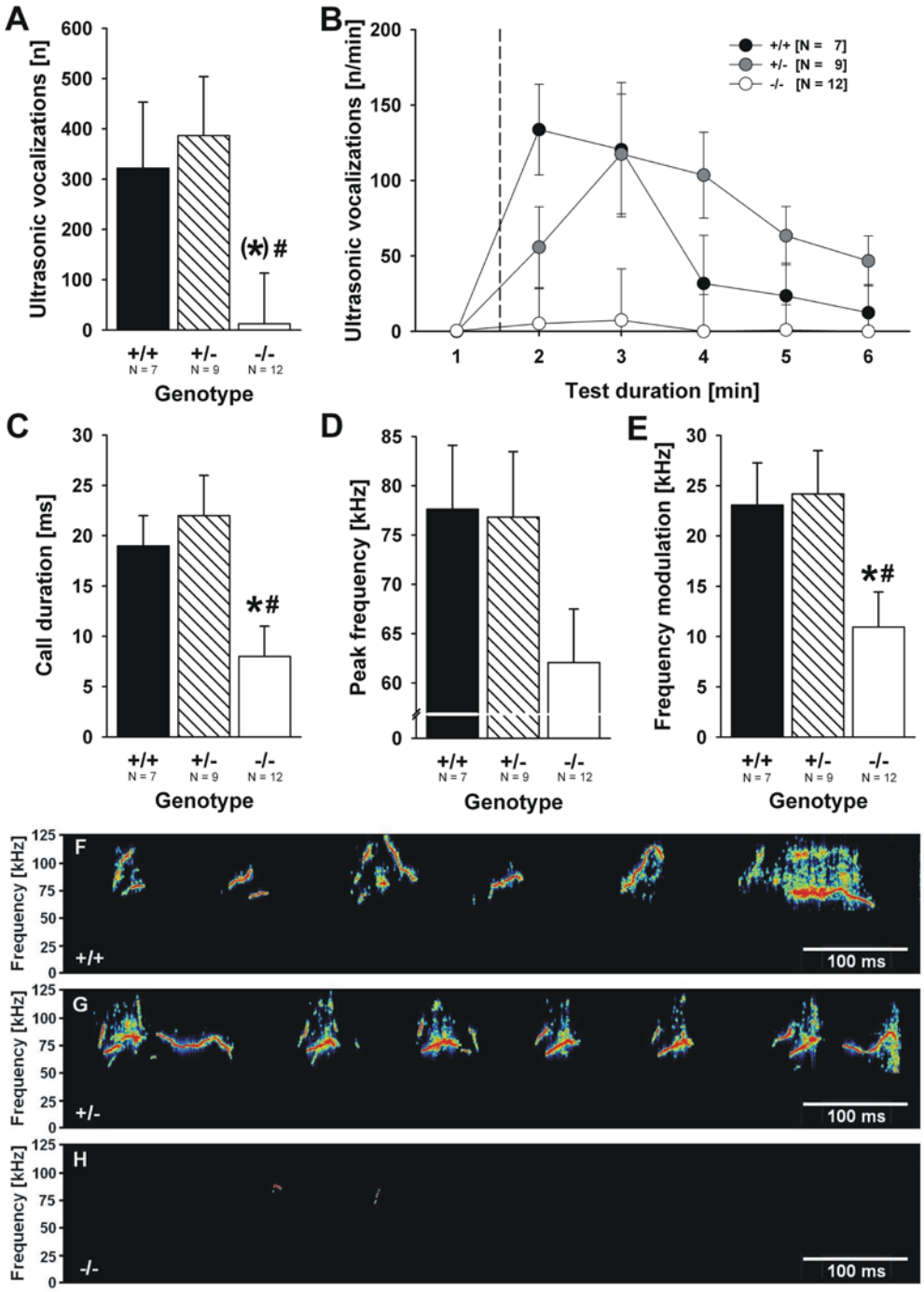

Supplementary Figure S2: Impairments in communication: PV$^{-/-}$ null mutant, but not PV$^{+/-}$ heterozygous mice display ultrasonic vocalization deficits during female exposure in adulthood. (A) Total number of ultrasonic vocalizations emitted during the 5 min female exposure period (genotype: $F_{2,24}$=3.417, p=0.049) (B) Time course for the number of

ultrasonic vocalizations emitted for each 1 min time bin across the 5 min female exposure period, plus 1 min habitation (dashed line indicates introduction of female mouse). (C) Duration of calls (genotype: $F_{2,24}$=5.302, p=0.014), (D) peak frequency (genotype: NS), and (E) frequency modulation of calls (genotype: $F_{2,24}$=3.789, p=0.040) emitted during the 5 min female exposure period. Black bar: $PV^{+/+}$ wildtype littermate control mice; striped bar: $PV^{+/-}$ heterozygous mice; white bar: $PV^{-/-}$ null mutant mice. Data are presented as means±SEM, bars denoting the SEM. * p<0.050 vs. $PV^{+/+}$; # p<0.050 vs. $PV^{+/-}$. (F-H) Representative spectrograms of ultrasonic vocalizations emitted during female exposure by (F) an adult $PV^{+/+}$ wildtype littermate control mouse, (G) an adult $PV^{+/-}$ heterozygous mouse, and (H) an adult $PV^{-/-}$ null mutant mouse.

Supplementary Figure S3

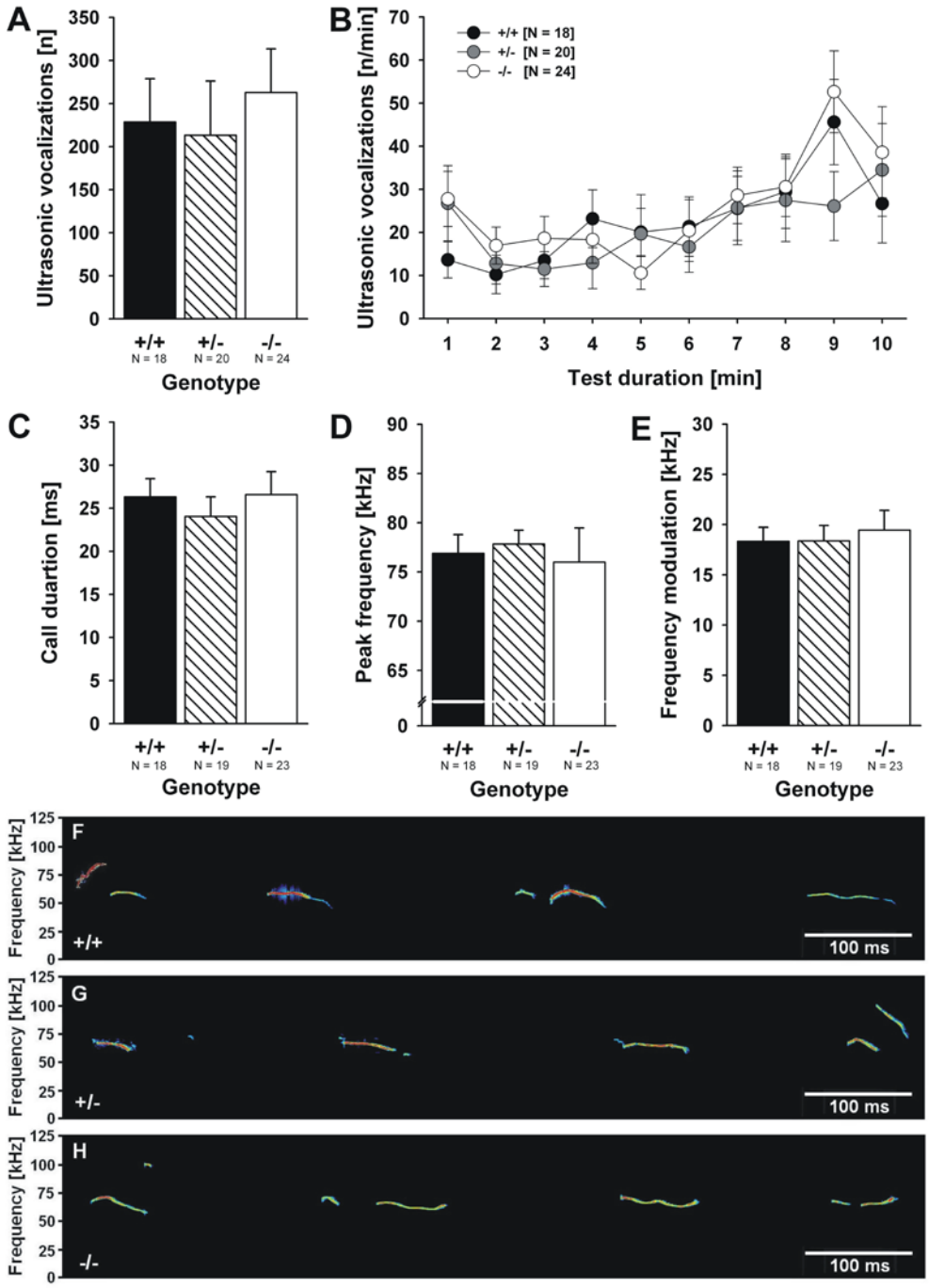

Supplementary Figure S3: No impairments in communication before PV expression starts: PV$^{-/-}$ null mutant and PV$^{+/-}$ heterozygous mice do not display ultrasonic vocalization deficits during social isolation as pups. (A) Total number of ultrasonic vocalizations emitted during the 10 min social isolation period (genotype: NS; sex: NS; genotype x sex: NS). (B) Time course for the number of ultrasonic vocalizations emitted for

each 1 min time bin across the 10 min social isolation period. (C) Duration of calls (genotype: NS; sex: NS; genotype x sex: NS), (D) peak frequency (genotype: NS; sex: NS; genotype x sex: NS), and (E) frequency modulation of calls (genotype: NS; sex: NS; genotype x sex: NS) emitted during the 10 min social interaction period. Black bar: $PV^{+/+}$ wildtype littermate control mice; striped bar: $PV^{+/-}$ heterozygous mice; white bar: $PV^{-/-}$ null mutant mice. Data are presented as means±SEM, bars denoting SEM. (F-H) Representative spectrograms of ultrasonic vocalizations emitted during pup social isolation by (F) a $PV^{+/+}$ wildtype littermate control mouse, (G) a $PV^{+/-}$ heterozygous mouse, and (H) a $PV^{-/-}$ null mutant mouse.

Supplementary Figure S4

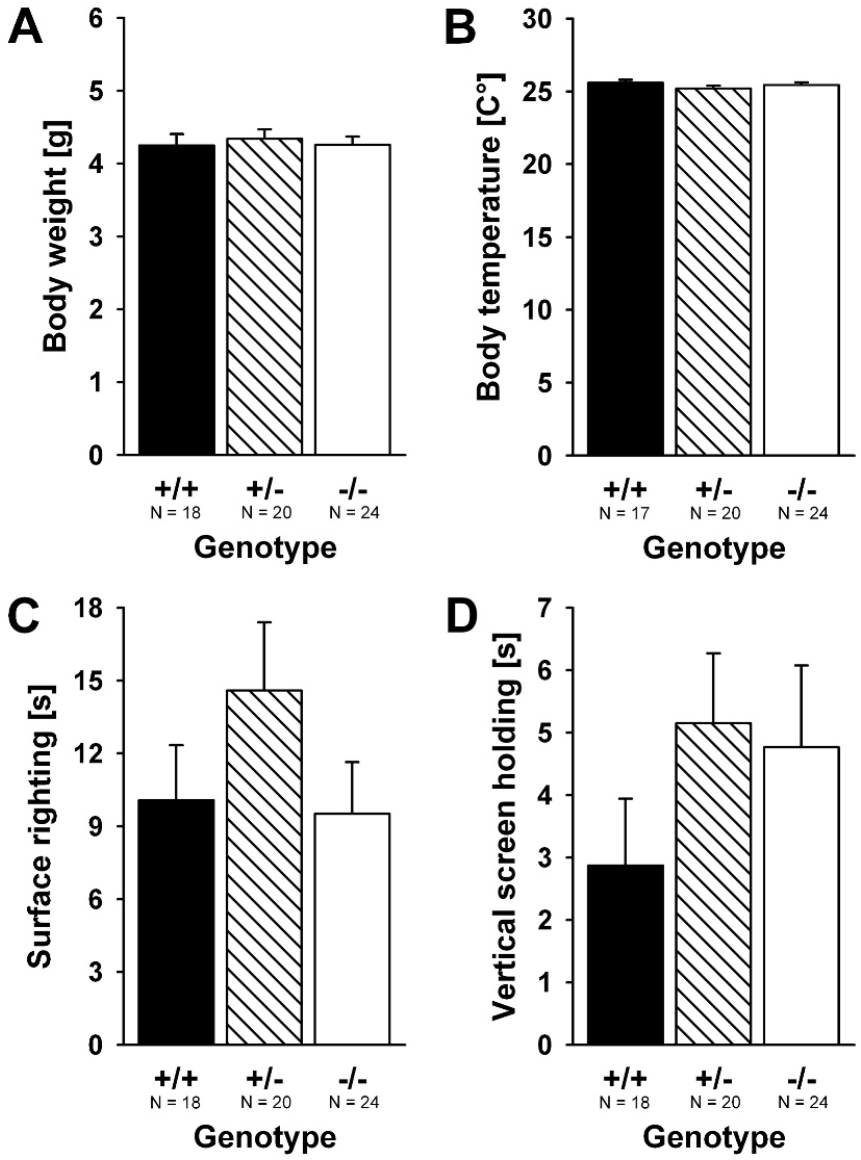

Supplementary Figure S4: No developmental alterations before PV expression starts: $PV^{-/-}$ null mutant and $PV^{+/-}$ heterozygous mice do not display developmental delays as pups. (A) Body weight, (B) body temperature, (C) surface righting, and (D) vertical screen holding on postnatal day 8. Black bar: $PV^{+/+}$ wildtype littermate control mice; striped bar: $PV^{+/-}$ heterozygous mice; white bar: $PV^{-/-}$ null mutant mice. Data are presented as means±SEM, bars denoting SEM.

Supplementary Figure

S5

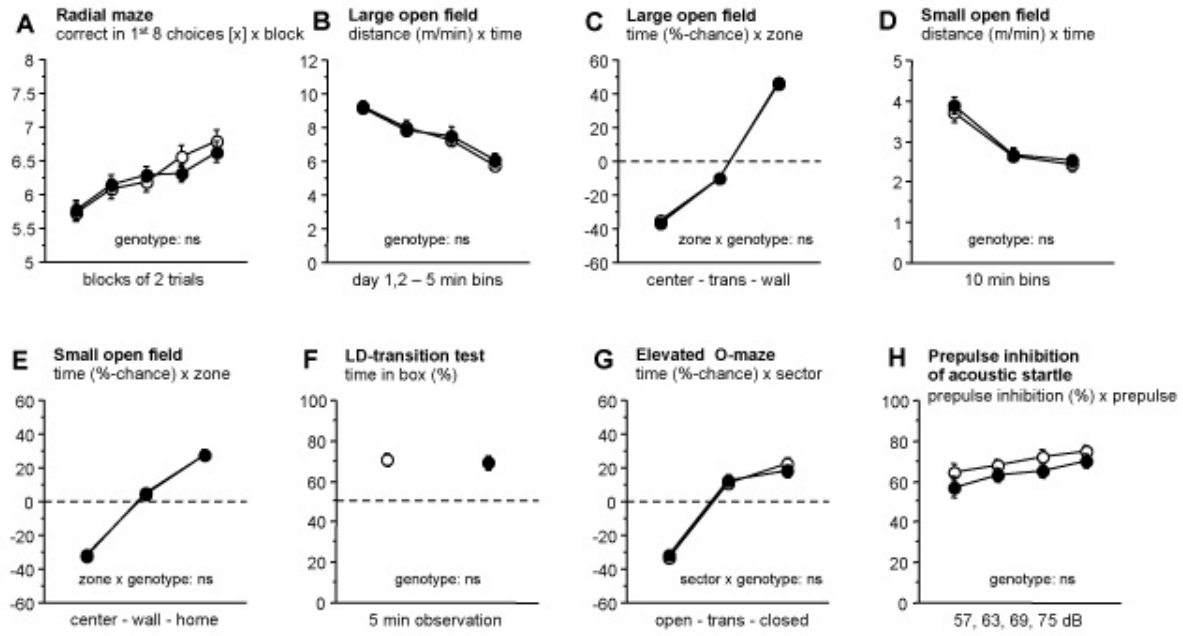

Supplementary Figure S5: **Normal memory as well as exploration and anxiety-related behaviors in PV$^{-/-}$ mice.** (A) Memory performance estimated as correct in 1st eight choices during 10 days of training. There was no mutation effect on performance or learning rate (genotype: $F_{1,56}$=0.0, NS; block: $F_{4,224}$=19.2, p<0.0001; block x genotype: $F_{4,224}$=0.9, NS). (B) In the large open-field, there was no mutation effect on activity level or habituation rate (distance moved normalized to 1 min observation time plotted in 5-min bins; ANOVA, genotype: $F_{1,52}$=0.5, NS; time: $F_{3,156}$=62.0, p<0.0001; time x genotype: $F_{3,156}$=0.5, NS). (C) In the same arena, center field avoidance was strong and unaffected by genotype (time in center field, transition and wall zone as % minus chance; ANOVA, zone: $F_{2,104}$=1299.6, p<0.0001; zone x genotype: $F_{2,104}$=0.3, NS). (D) Also in the small open-field with home box, there was no mutation effect on activity level or habituation rate (distance moved normalized to 1 min observation time plotted in 10-min bins; ANOVA, genotype: $F_{1,27}$=0.2 NS; time: $F_{2,54}$=124.5, p<0.0001; time x genotype: $F_{2,54}$=0.3, NS). (E) In the same arena, center field avoidance was strong and unaffected by genotype (time in center field, wall zone and home box area as %-

chance; ANOVA, zone: $F_{2,56}$=267.1, p<0.0001; zone x genotype: $F_{2,56}$=0.0, NS). (F) In the light-dark transition test, both groups spent a similar amount of time inside the box (time in box; ANOVA, genotype: $F_{1,27}$=0.1, NS; 1-sample t-test vs. change p<0.001). (G) Both groups showed similarly strong avoidance of the open sectors of the elevated O-maze (time on open sectors, transition zones and closed sectors as %-chance; ANOVA, sector: $F_{2,56}$=175.8, p<0.0001; sector x genotype: $F_{2,56}$=0.6, NS). (H) Prepulse inhibition of the startle response to a 120 dB white noise stimulus. There was no significant mutation effect (genotype: $F_{1,28}$=1.6, NS; prepulse: $F_{3,84}$=18.1, p<0.0001; prepulse x genotype: $F_{3,84}$=0.4, NS). Data are presented as means±SEM, bars denoting SEM.

Supplementary Figure S6

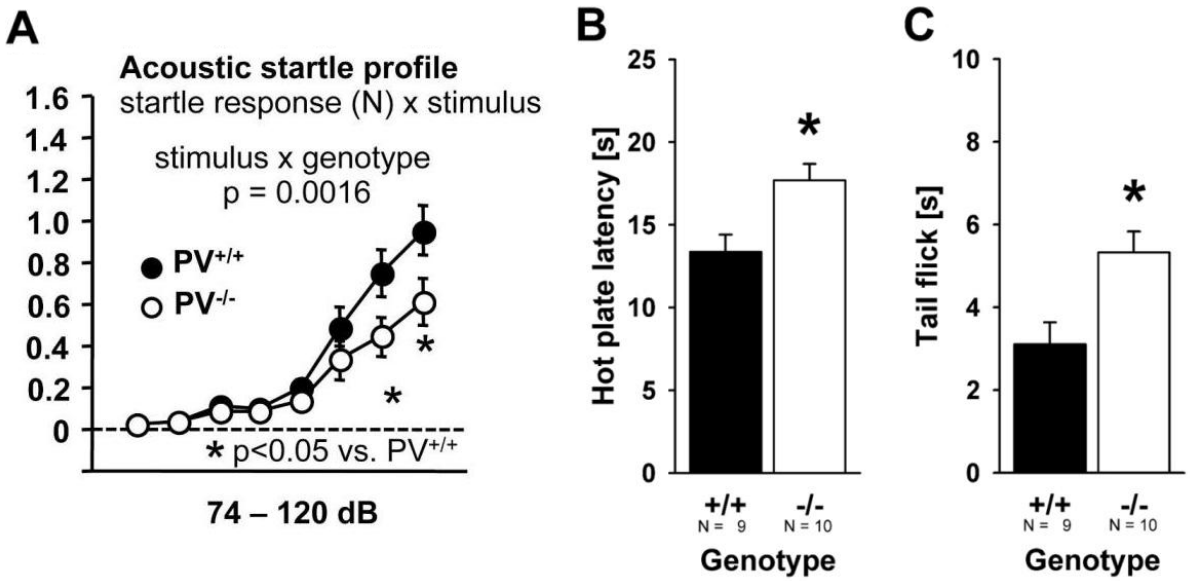

Supplementary Figure S6: Acoustic startle response (ASR) and nociception. (A) Acoustic startle response to white noise stimuli of 74, 78, 82, 86, 90, 100, 110 and 120 dB. The ASR amplitude is measured in mV. $PV^{-/-}$ showed weaker responses at 110 and 120 dB (genotype: $F_{1,28}$=5.0, p=0.033; sound pressure level of stimulus: $F_{7,196}$=55.7, p<0.0001; sound pressure level of stimulus x genotype: $F_{7,196}$=3.5 p=0.0016; * p<0.05 vs. $PV^{+/+}$). (B) $PV^{-/-}$ mice displayed a delayed reaction time in the hot plate test (genotype: p<0.02). (C) Similarly, reaction times were also delayed in the tail flick test in $PV^{-/-}$ mice (genotype: p<0.01), with no significant difference in body weight between $PV^{+/+}$ and $PV^{-/-}$ animals (data not shown). ANOVA including genotype and sex: * p<0.005. Data are presented as means±SEM, bars denoting the SEM.

Supplementary Figure S7

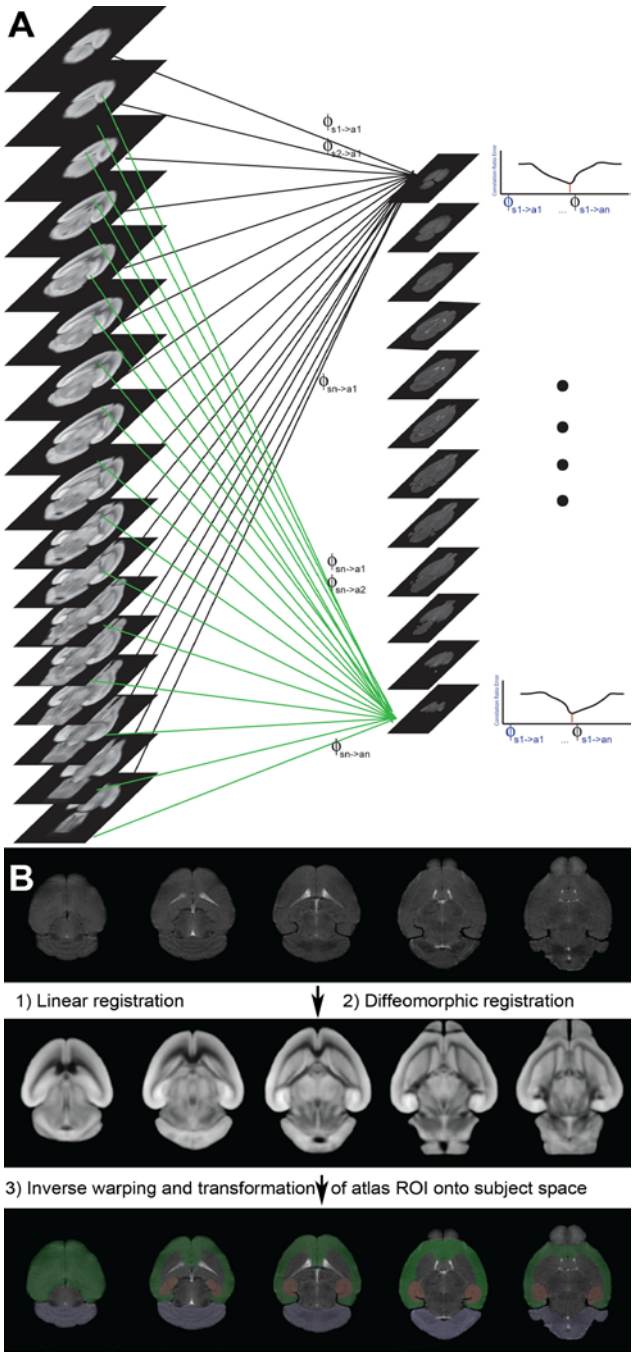

Supplementary Figure S7: Methods used for semi-automated selection of regions of interest (ROIs). A) Shown are the P0 template atlas (left) and the source T2 volumes (middle), which were co-registered using (FLIRT, see methods) the function is shown to the right. (Φ represent best scores to a transformed source slice). B) Representative examples of

the steps required to obtain labeled ROIs: neocortex (green); cerebellum (purple) and hippocampus (red).

Supplementary Figure S8

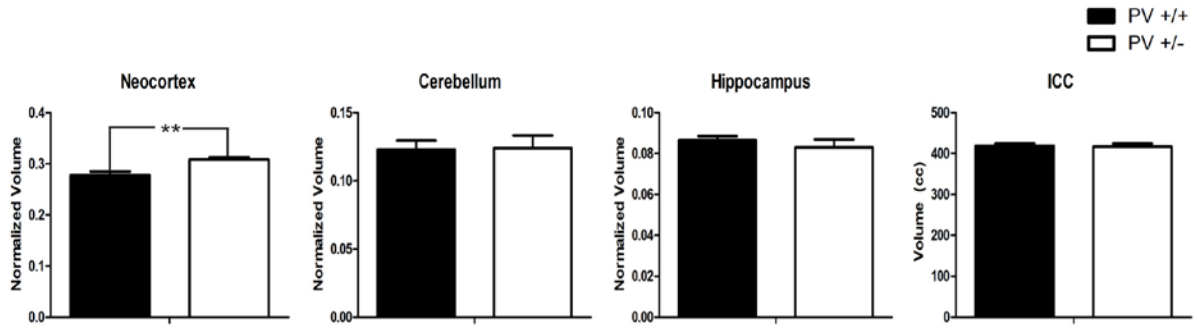

Supplementary Figure S8: Neocortical volume is increased in male juvenile (PND20) heterozygous ($PV^{+/-}$) mice. Shown are neocortical, cerebellar and hippocampal volumes, all normalized to intracranial content, from $PV^{+/+}$ and $PV^{+/-}$ mice (fixed brains with intact cranium). The neocortical volume in $PV^{+/-}$ was significantly larger ($F_{1,11}$=12.24, p=0.007), while cerebellar and hippocampal volumes were not significantly different ($F_{1,11}$=0.14 p=0.909 and $F_{1,11}$=0.22 p= 0.645 respectively), intracranial volumes did not vary either ($F_{1,11}$=0.064; p=0.805). Data are presented as means±SEM, bars denoting the SEM. ** p<0.01.

Supplementary Figure S9

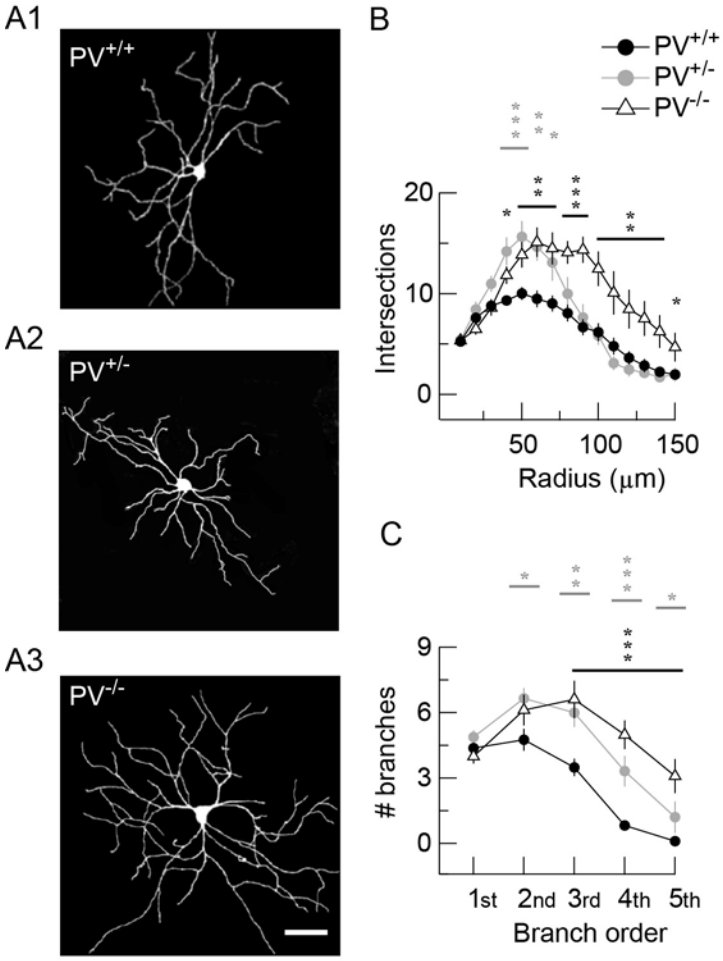

Supplementary Figure S9: Increased dendritic branching in $PV^{-/-}$ and $PV^{+/-}$ FSI. (A1-A3) Representative confocal projections of a biocytin-loaded $PV^{+/+}$, $PV^{+/-}$ and $PV^{-/-}$ FSI. (B) Sholl analysis: values represent the number of dendrites crossing concentric rings drawn at 10-μm intervals from the FSI soma. At radial distances between 40 to 150 μm from the soma, $PV^{-/-}$ neurons (n=8) presented a significant increase in the number of dendrites compared to the $PV^{+/+}$ counterparts (n=18). In $PV^{+/-}$ FSI (n=9), the increase in branching was restricted to a zone of 40-70 μm from the soma. (C) Pooled values depicting the number of first, second, third, fourth and fifth order dendritic branches of the same FSI analyzed in B. The increased number of dendrites in the $PV^{-/-}$ group results from an increase in terminal branches of third,

198 fourth and fifth order compared to controls; for $PV^{+/-}$ FSI this additionally comprises second
199 order branches. Scale bar: 50 μm, for all images in A. All values are presented as
200 means±SEM, bars denoting the SEM. * $p<0.05$, ** $p<0.01$, *** $p<0.001$; for PV-reduced
201 ($PV^{+/-}$; gray symbols) and PV-devoid (white symbols) FSI vs. WT ($PV^{+/+}$), Student's t test.